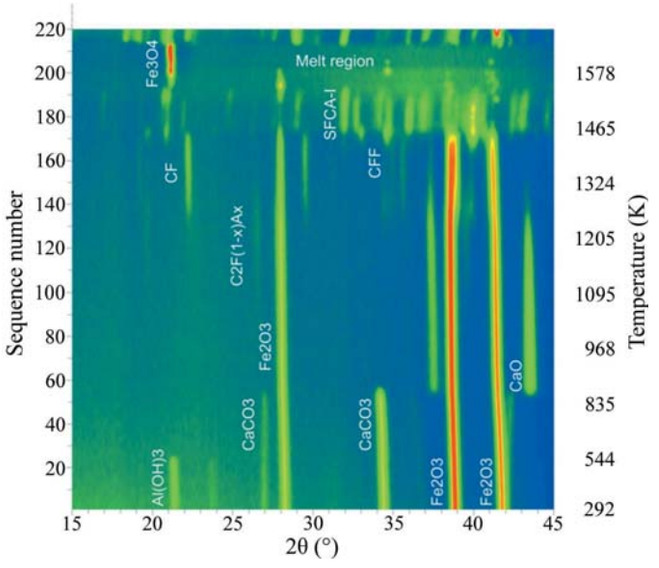

Figure 3.9.14
Raw *in situ* XRD data (Co $K\alpha$ radiation) collected during the synthesis of the iron-ore sinter bonding phase SFCA-I (Webster *et al.*, 2013). The data, collected as a function of heating temperature, are viewed down the intensity axis with red representing the highest intensity and blue the lowest intensity. The identified phases include gibbsite $Al(OH)_3$, calcite $CaCO_3$, haematite Fe_2O_3, lime CaO, calcium ferrites CF and CFF, calcium alumina-ferrite $C_2F_{1-x}A_x$, magnetite Fe_3O_4, and SFCA-I.

sinter bonding phase, SFCA-I, where SFCA = silico-ferrite of calcium and aluminium (Scarlett, Madsen *et al.*, 2004; Scarlett, Pownceby *et al.*, 2004; Webster *et al.*, 2013). The starting material, comprising a synthetic mixture of gibbsite, $Al(OH)_3$, haematite, Fe_2O_3, and calcite, $CaCO_3$, was heated to about 1573 K using an Anton Paar heating stage. The laboratory-based XRD data, collected using an Inel CPS120 diffractometer, are shown in Fig. 3.9.14, while the QPA results are shown in Fig. 3.9.15. Both figures show that there are several phase changes, including the formation of transient intermediate phases before the final production of SFCA.

In Fig. 3.9.15(*a*) the QPA results are derived using the Hill/Howard algorithm (Hill & Howard, 1987) in equation (3.9.26): this is the 'default' value reported by most Rietveld analysis software and normalizes the sum of the analysed components to 100 wt%. The apparent increase in haematite concentration at about 533 and 868 K results from the decomposition of gibbsite and calcite, respectively. There are no possible mechanisms in this system that could lead to an increase in haematite concentration at these temperatures; the reported increases are an artefact derived from normalizing the sum of all analysed phases to 100 wt%. Fig. 3.9.15(*b*) shows the correct result derived using the external-standard approach (O'Connor & Raven, 1988) embodied in equation (3.9.21), which has placed the values on an absolute scale. Fig. 3.9.15 demonstrates the importance of putting the derived phase abundances on an absolute scale for a realistic derivation of reaction mechanism and kinetics.

3.9.8. QPA using neutron diffraction data

One of the early papers detailing the application of the Rietveld method to quantitative phase analysis used neutron diffraction (ND) data (Hill & Howard, 1987). The reasons stated within this work define many of the advantages of neutrons over X-rays for diffraction in general and QPA in particular. One of the most significant advantages for QPA derives from the fact that neutrons interact weakly with matter, hence there is very little microabsorption with ND even in samples comprising a mixture of high- and low-atomic-number materials.

The high penetration capability of neutrons also enables the use of larger sample environments in *in situ* studies, thus enabling studies to be undertaken at, for example, higher pressures than would be possible with many X-ray sources. In addition, larger sample volumes can be investigated, which in turn produces better particle statistics and makes the technique less sensitive to grain size. It also makes ND a bulk technique in comparison with XRD, which is effectively surface-specific with a penetration depth of the order of microns or tens of microns.

The different strengths of ND and XRD mean that they can be exploited in combination to provide complementary information. For example, XRD generally has higher angular resolution and is therefore better at resolving small lattice distortions and heavily overlapped phases. However, the observed intensities in ND do not decrease as strongly with decreasing d-spacing. This results in ND providing more accurate determination of atomic displacement parameters and therefore the Rietveld scale factors; this then improves the accuracy of QPA derived from these scale factors (Madsen *et al.*, 2011).

Hill *et al.* (1991) have investigated the phase composition of Mg-PSZ (partially stabilized zirconia) using both ND and XRD. The surfaces of these materials were subjected to various treatments, which meant that they were no longer representative of the bulk. From the more highly penetrating ND data they obtained bulk properties including crystal structure and size and strain parameters of the components along with QPA. From XRD they were able to examine the surface of the samples to investigate the effects of surface grinding and polishing.

The majority of Rietveld-based QPA still relies on the use of accurate crystal structure models; consequently, it is of increasing importance that powder diffraction methods used for structure solution be robust and reliable. Combining laboratory or synchrotron XRD and ND has been shown to be of considerable benefit in the solution of complex structures *via* powder diffraction (Morris *et al.*, 1992). This joint-refinement approach has been used to determine the crystal structure of a component phase of Portland cement (De La Torre *et al.*, 2002) for subsequent use in Rietveld-based QPA.

One of the disadvantages of neutron sources is that they are much less accessible than laboratory X-ray sources and of much lower flux than either laboratory or synchrotron X-rays sources. In addition, larger samples are generally required; this is not always practical in the investigation of many materials.

In many phase systems, the presence of severe microabsorption in XRD data serves to limit the accuracy that can be obtained. The collection of ND data, where microabsorption is virtually absent, from selected samples provides more accurate QPA; selected ND-based values can therefore act as a benchmark for the more routine XRD-based studies.

3.9.9. QPA using energy-dispersive diffraction data

Energy-dispersive diffraction (EDD) involves the use of high-energy white-beam radiation, often from a synchrotron source. This provides very high penetration and is, therefore, ideal as a probe to examine the internal features of relatively large objects (Barnes *et al.*, 2000; Cernik *et al.*, 2011; Hall *et al.*, 1998, 2000). In an experimental arrangement such as that in Fig. 3.9.16, diffraction data can be measured by energy-dispersive detec-